Detection of Vortices and Saddle Points in SST Data*

Q. Yang and B. Parvin
Imaging and Collaborative Computing
Computing Sciences
Lawrence Berkeley National Laboratory
Berkeley, CA 94720

A. Mariano
RSMAS
University of Miami
4600 Rickenbacker Causeway
Miami, FL 33149

September 19, 2000

Abstract

We extend the Horn-Schunck model of flow field computation to incorporate incompressibility for tracking fluid motion. This is expressed as a weak form of zero-divergence constraint in the variational problem and implemented with a multigrid approach for efficient computation. The resulting feature displacement velocity field provides the basis for higher level abstraction and representation of the data for data mining. A robust and efficient algorithm, based on the Jordan curve index, for detecting vortices and saddle points in feature displacement fields derived from sequences of satellite-derived SST fields is presented.

1 Introduction

The detection and tracking of coherent flow features in oceanographic data, especially vortices such as Gulf Stream rings, are an important scientific tasks because these features are efficient transport and mixing mechanisms for salt/freshwater, heat, plankton communities, and nutrients (*e.g.,* Iselin [10]; Ichiye [9]; Nowlin [17]; Lai and Richardson [13]; Richardson [20]; Olson [18]). Earlier studies relied on detecting thermal and/or salinity anomalies in hydrographic surveys (Lindstrom and Taft [15]). Other studies detected rotary motion in the trajectories of surface drifters/subsurface floats (Kirwan *et al.* [12]; Richardson [21]), identified well-defined anomalies in satellite images (Brown *et al.* [4]), or calculated feature displacement velocities using a sequence of images and then manual identification of coherent circulation features (Kelly [11]; Emery *et al.* [6]). Here, we introduce a new formulation of flow field computation that incorporates a weak constraint for incompressibility for tracking fluid motion. The proposed technique is then implemented through a multigrid representation to reduce the computational complexity. Coherent features in the flow field, such as vortices and saddle points, are automatically identified using the Jordan curve index.

*This work is supported by the Director, Office of Energy Science Research, Office of Computation and Technology Research, Mathematical, Information, and Computational Sciences Division of the U. S. Department of Energy under Contract No. DE-AC03-76SF00098 with the University of California. LBNL publication number is 44711. Arthur J. Mariano was supported by the Office of Naval Research under Grant N00014-95-1-0257.

Results using sequences of satellite-derived sea surface temperature fields are presented. These data are processed, calibrated, composited, and derived from AVHRR data from the NOAA satellites at the University of Miami and then sent to Berkeley for feature analysis.

In Section 2, we review previous work in flow fields computation and subsequent feature extraction. Section 3 provides the details of our approach, including flow computation, feature detection, and experimental results on real data. Section 4 concludes the paper.

2 Previous Work

This section briefly reviews previous research in tracking of fluid motion and related work in feature extraction from the vector field. Measurement and analysis of feature velocities are often referred to as computation of optical flow in the imaging literature. Review and enhancement of these techniques can be found in [3, 14]. However, tracking fluid motion poses additional constraints that have been addressed by only a few papers. In this context, we are not interested in tracking compressible fluid that focuses on clouds and images obtained from turbulent flows [16, 23]. These systems pose an affine model over the time-varying imagery and ignore the inherent incompressibility constraint.

Cohen and Herlin [5] proposed a nonquadratic regularization technique for solving the optical flow constraint equation and applied it to oceanographic images. Their approach applies to irregularly spaced images with missing data. The regularization problem was solved by finite difference methods with finer tessellation near the motion boundary. Their method does not incorporate any constraints imposed by the fluid motion. Amini [1] extended the Horn-Schunck equation to include fluid X-ray images of contrast velocity in arteries. This was expressed in terms of zero divergence of flow field to *simplify* the solution. A major drawback of his approach is that the corresponding partial differential equations are of a higher order.

Raw oceanic data consist of satellite swath data and artifacts introduced by clouds. Modern oceanic processes perform cloud removal and time-space interpolation to produce dense data for daily, regional, and global fields. These data are then calibrated with in-situ measurements to produce a dense temperature map at each point on the oceanic grid. Dense oceanic data are the starting point for the proposed analysis that should satisfy the fluid incompressibility constraint. Additionally, because the data reside in the spherical coordinate system, special treatment is needed. Our formulation operates on dense data, does not require solution of higher order PDEs, and it has been implemented in a multigrid framework for better computational efficiency.

With respect to feature extraction from the vector field, previous approaches rely on eigenvalue analysis from the local Jacobian [19, 22]. Our experience indicates that feature extraction is highly dependent on the smoothness of flow computation. If the flow field is regularized (as it is in our case), then events of interest can be easily localized. We will present an elegant approach for detection of vortices and saddle points that has proved to work effectively in our data sets.

3 Approach

In this section, we will describe a set of algorithms to compute feature velocities from consecutive images of sea surface temperature data and to localize singular events (saddle points and vortices) from velocity vectors.

3.1 Computation of feature velocities

Let $I(x, y, t)$ be the image at time t, with (u, v) as the velocity vector at each point. The flow field equation with brightness constancy assumption is given by:

$$\frac{dI(x,y,t)}{dt} = I_x u + I_y v + I_t = 0 \tag{1}$$

where the subscripts x, y, and t represent the partial derivatives. Horn and Schunck [8] constrained the problem by incorporating local smoothness in the flow. This paper extends their model by adding the incompressibility constraint (zero divergence) in a weak sense. At each point, the zero-divergence is given by $u_x + v_y = -w_z$; however, our model enforces incompressibility only along the temperature gradient (normal to isothermals), e.g., $u_x + v_y = 0$. The full model is given by:

$$\begin{aligned} (u^*_\beta, v^*_\beta) &= arg \min E := \tfrac{1}{2} \int \int [(I_x u + I_y v + I_t)^2 \\ &+\alpha(|\nabla u|^2 + |\nabla v|^2) + \beta(u_x + v_y)^2] dx dy \end{aligned} \tag{2}$$

where α and β are the weighting factors for enforcing smoothness and incompressibility constraints. Note that spherical coordinates should be used in this equation. The Euler-Lagrange equation of this equation is

$$\begin{aligned} -I_x(I_x u + I_y v + I_t) + (\alpha + \beta) u_{xx} + \alpha u_{yy} + \beta v_{xy} &= 0 \\ -I_y(I_x u + I_y v + I_t) + \alpha v_{xx} + (\alpha + \beta) v_{yy} + \beta u_{xy} &= 0 \end{aligned} \tag{3}$$

which can be solved using finite difference approximation. The algorithm is iterative and converges to a local minimum solution, satisfying smoothness and a zero-divergence weak constraint. The solution to the above equations is achieved through multigrid technique to reduce the computational complexity. Let h be the window size where finite differences are computed. Then by setting $h = 2^K, 2^{K-1}, \cdots, 1$ successively, we can propagate from coarse to fine grid through simple linear interpolation and refinement.

3.2 Multigrid approach

The solution to the above equations is achieved through multigrid technique to reduce the computational complexity. Let h be the window size where finite differences are computed. Then by setting $h = 2^K, 2^{K-1}, \cdots, 1$ successively, we can propagate from coarse to fine grid through simple linear interpolation and refinement. Linear interpolation is used because motion is locally smooth. It simply sets an initial condition for higher resolution computation to take place. This multigrid method can be described as follows:

- STEP 0. $h = 2^K$
- STEP 1. Repeat the following algorithm until it converges:

  for $(i = 0; i < M; i = i + h)$

for $(j=0; j<N; j=j+h)$ let

$$\begin{cases} u_{j,i} = \frac{1}{D}[(I_y^2 + \frac{4\alpha+2\beta}{h^2})\Delta_1^{(n)} - IxIy\Delta_2^{(n)}] \\ v_{j,i} = \frac{1}{D}[-IxIy\Delta_1^{(n)} + (I_x^2 + \frac{4\alpha+2\beta}{h^2})\Delta_2^{(n)}] \end{cases}$$

where $M \times N$ is the image size.

- STEP 2. Linear interpolation

  for $(i=0; i<M; i++)\{$

  $i_0 = [i/h]\cdot h, r_i = (i-i_0)/h;$

  for $(j=0; j<N; j++)$ $\{$

  $j_0 = [j/h]\cdot h, r_j = (j-j_0)/h;$

  $$u_{j,i} = (1-r_i)(1-r_j)u_{j_0,i_0} + r_i(1-r_j)u_{j_0,i_0+h} + (1-r_i)r_j u_{j_0+h,i_0} + r_i r_j u_{j_0+h,i_0+h}$$
  $$v_{j,i} = (1-r_i)(1-r_j)v_{j_0,i_0} + r_i(1-r_j)v_{j_0,i_0+h} + (1-r_i)r_j v_{j_0+h,i_0} + r_i r_j v_{j_0+h,i_0+h}$$

  $\}$

  $\}$

- STEP 3. If $h=1$, stop; else $h=h/2$, goto STEP 1.

Note that in STEP 1, all the pixels are updated asynchronously and not simultaneously. Why is the asynchronous iteration faster than the synchronous? An intuitive explanation is that the pixels that have been updated will be used to update their neighborhood. Even though this idea is rather simple, it can speed up the convergence greatly. In fact, it is a deterministic version of the classic Gibbs sampler [7].

3.3 Evaluation of feature velocities

Both α and β of the regularization parameters are important for correct measurement of feature velocities. The corresponding difference operators are weighted to take into account the fact that observed values are in the spherical, S^2, as opposed to the Cartesian coordinate system, R^2. We have compared our measurements with ground truth data (obtained from surface drifters) and verified that our measurements are consistent. For example, from Nov. 5, 1986, to Nov. 18, 1997, Aoki et al. [2] indicated a motion field of 3-5cm/sec to the west from 35° to 40° N in the region 30° to 40° N and 140° E to 170° W. Our measurements in the same area indicate a motion of 3.0 to 3.5 cm/sec.

Our method has been applied to AVHRR data at 18 Km spatial and 48 hours temporal resolution. We have processed all the data from 1986 to 1998. The feature based statistical analysis will soon be published in a companion paper. The average execution time for computing feature velocities, vortices, and saddle points is about 2 minutes per image on a Sun Ultra 60 running at 330 MHz. The code was written in C++, and it can be further optimized.

3.4 Detection of vortices and saddle points

Singularities in the flow field can provide a compact abstraction in the velocity field. This issue has been addressed in literature [19], where an algorithm based on the analysis of local Jacobian was proposed. Their approach is complex because the flow field is not regularized. Here, we propose an alternative method for robust estimation of event detection and subsequent tracking of singularities.

Let $F = (u, v)$ be a vector field and J be a Jordan curve with no critical point on it. The index of J is defined by

$$\text{Index}(J) = \frac{1}{2\pi} \oint_J \frac{udv - vdu}{u^2 + v^2} \tag{4}$$

At each point P, we choose a small circle J_P around P and compute Index(J_P). The flow field (u, v) can then be classified according to:

1. The index of a vortex is equal to $+1$ (the classification of singular points in a vector field is given in [19]), and
2. The index of a saddle point is equal to -1.

There is no node in the vector field because of the zero-divergence constraint, but singularities do occur. Recall that a point (x, y) is singular iff $u(x, y) = 0$ and $v(x, y) = 0$. However, using this condition to localize singularities leads to computational instability. A better approach is to exploit the inherent local minimum velocity volume to simplify the problem. Thus,

- Step 1: Find all local minima of the velocity field, i.e., $\sqrt{u(x,y)^2 + v(x,y)^2}$
- Step 2: $\forall (x, y) \in S$:

  (1) Let $R = \frac{1}{2}\max\{r | S \bigcap J^r_{(x,y)} = \phi\}$ where $J^r_{(x,y)}$ is the circle centered at (x, y) with radius r.
  (2) Compute the index of $J^R_{(x,y)}$, that is,

$$\text{Index}(J^R_{(x,y)}) = \frac{1}{2\pi} \oint_{J^R_{(x,y)}} \frac{udv - vdu}{u^2 + v^2} \tag{5}$$

  (3) If Index$(J^R_{(x,y)}) = 0$, then (x, y) is not singular; if Index$(J^R_{(x,y)}) = 1$, then (x, y) is a vortex; if Index$(J^R_{(x,y)}) = -1$, then (x, y) is a saddle point.

An example of saddle points, observed in the Pacific, is shown in Figure 1. This image indicates that saddle points are not rare and that they occur often in the oceanic flow. One important characteristic of vortex is its "size." Here, we propose a simple definition. If a point (x, y) is a vortex, then its size $R^*(x, y)$ can be defined as:

$$R^*(x, y) = \max\{R | \text{Index}(J^R_{(x,y)}) = 1\} \tag{6}$$

that is to say, $R^*(x, y)$ is the largest R such that the index of $J^R_{(x,y)}$ remains 1.

Fig. 2 shows the feature velocities, vortices, and saddle points corresponding to a pair of SST data on day 200 of the year 1992. The arrows show the direction of feature velocities, the underlying intensity shows the magnitude of velocity, vortices and their size are indicated by a red block and blue circle, and saddle points are shown with a green block. It is interesting to note that saddle points are an integral component of the oceanic dynamic.

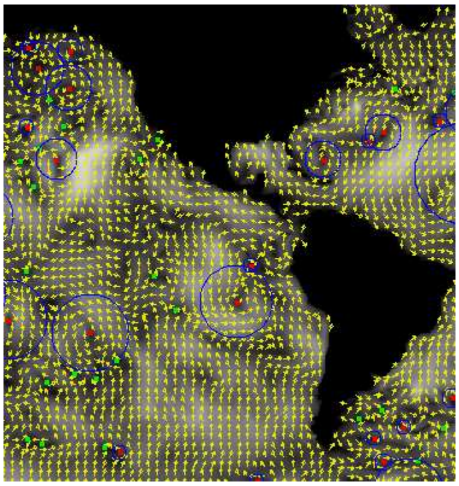

Figure 1: Feature velocity of SST (in yellow), magnitude of velocity (encoded with the underlaying intensity), vortices and their size (in red block with blue circle for size), and saddle points (in green) on the 100th day of 1992.

4 Conclusions

In this paper, we formulated motion computation in oceanographic images as a constrained variational problem with incompressibility constraint, which is a generalization of Horn-Schunck's original work. A robust technique for detection of singularities (vortices and saddle points) in the velocity field was proposed, implemented, and shown on real data. We showed the effectiveness of our approach at mesoscale. Our aim is to continue using these events for high level representation of large-scale geophysical data, reconstruction of high-resolution SST data, and subsequent data mining.

References

[1] A.A. Amini. A scalar function formulation for optical flow: Application to x-ray imaging. In *IEEE Workshop on BioMedical Imaging*, pages A:117–124, 1994.

[2] S. Aoki, S. Imawaki, and K. Ichikawa. Baroclinic disturbances propagating westward in the kuroshio extension region as seen by a satellite altimeter and radiometers. *Geophysical Research-Oceans*, 100:839–855, 1995.

[3] J.L. Barron, D.J. Fleet, and S.S. Beauchemin. Performance of optical flow techniques. In *CVPR92*, pages 236–242, 1992.

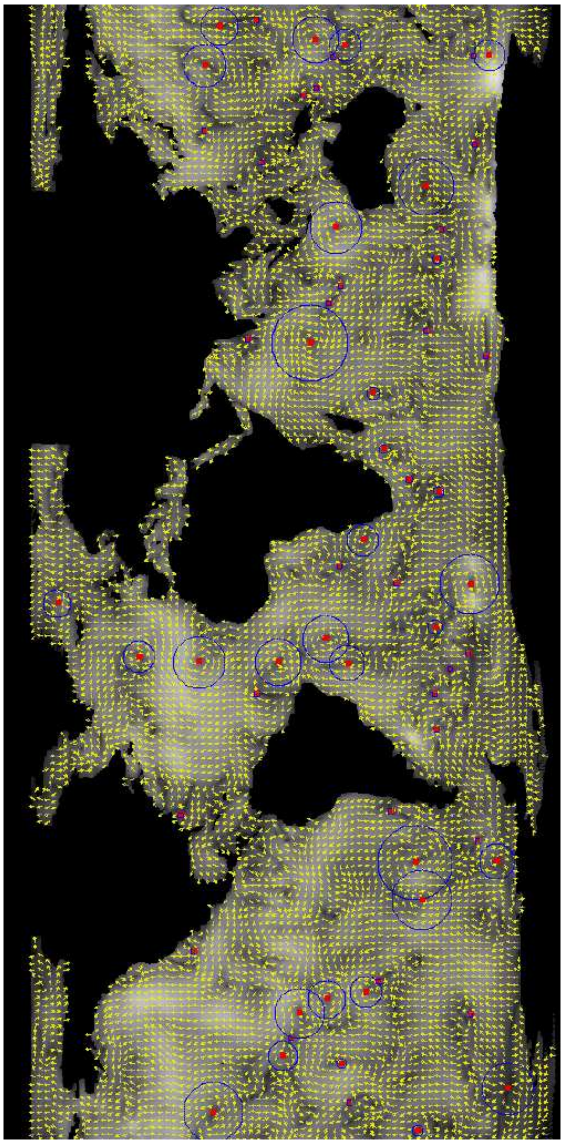

Figure 2: Feature velocities and computed vortices from SST: Feature directions are shown with arrows, and their corresponding magnitudes are shown with the underlying brightness map. Vortices are surrounded with a blue circle. This result is generated from a pair of consecutive images around day 200 from 1992.

[4] O.B. Brown, P.C. Cornillon, S.R. Emmerson, and H.M. Carle. Warm core rings: A statistical study of their behavior. *Deep-Sea Research*, 33:1459–1473, 1986.

[5] I. Cohen and I. Herlin. A motion computation and interpretation framework for oceanographic satellite images. In *SCV95*, pages 13–18, 1995.

[6] W.J. Emery, C. Fowler, and C.A. Clyson. Satellite-image-derived Gulf Stream currents compared with numerical model results. *J. of Atmospheric and Oceanic Technology*, 9:286–305, 1992.

[7] S. Geman and D. Geman. Stochastic relaxation, gibbs distribution and bayesian restoration of images. *PAMI*, 6:721–741, 1984.

[8] B. K. P. Horn and B. G. Schunck. Determining optical flow. *Artificial Intelligence*, 17:185–203, 1981.

[9] T Ichiye. On the behavior of the vortex in the polar front region. *Oceanography*, 8:115–132, 1955.

[10] C. Iselin. Preliminary report on long-period variations in the transport of the Gulf Stream system. *Papers in Physical Oceanography and Meteorology*, 8:1–40, 1940.

[11] K.A. Kelly. An inverse model for near-surface velocity from infrared images. *Physical Oceanography*, 19:1845–1864, 1989.

[12] A.D. Kirwan, Jr. Merrell, J.K. Lewis, R.E. Whitaker, and R. Legeckis. A model for the analysis of drifter data with an application to a warm core ring in the Gulf of Mexico. *J. Geophysical Research*, 89:3425–3438, 1984.

[13] D.Y. Lai and P.L. Richardson. Distribution and movement of Gulf Stream rings. *J. Physical Oceanography*, 7:670–683, 1977.

[14] S.H. Lai and B.C. Vemuri. Robust and efficient algorithms for optical flow computation. In *SCV95*, pages 455–460, 1995.

[15] E.J. Lindstrom and B.A. Taft. Small water-property transporting eddies: Statistical outliers in the hydrographic data of the polymode local dynamics experiment rings. *J. Physical Oceanography*, 16:613–631, 1986.

[16] M. Maurizot, P. Bouthemy, and B. Delyon. 2d fluid motion analysis from a single image. In *CVPR'98*, pages 184–189, Santa Barbara, California, 1998.

[17] W.D. Nowlin, J.M. Hubertz, and R.O. Reid. A detached eddy in the Gulf of Mexico. *Marine Research*, 26:185–186, 1968.

[18] D.B. Olson. Rings in the ocean. *Annual Review of Earth Planetary Science*, 19:283–311, 1991.

[19] A. R. Rao and R. C. Jain. Computerized flow field analysis: Oriented texture fields. *IEEE Transactions on Pattern Analysis and Machine Intelligence*, pages 693–709, 1992.

[20] P.L. Richardson. *Eddies in Marine Science.* Berlin: Springer-Verlag, 1983.

[21] P.L. Richardson. A census of eddies observed in north Atlantic sofar float data. *Prog. Oceanography*, 31:1–48, 1993.

[22] Y.L. Xiong and S.A. Shafer. Dense structure from a dense optical flow sequence. In *Intl. Symposium on Computer Vision*, pages 1–6, Coral Gables, Florida, 1995.

[23] L. Zhou, C. Kambhamettu, and D. Goldgof. Extracting nonrigid motion and 3d structure of hurricanes from satellite image sequences without correspondences. In *CVPR'99*, pages 281–285, Fort Collins, Colorado, 1999.